Computer Physics Communications 291 (2023) 108829

Contents lists available at ScienceDirect

Computer Physics Communications

journal homepage: www.elsevier.com/locate/cpc

Computational Physics

Implementation and verification of a model linearized multi-species collision operator in the COGENT code ☆

A.R. Knyazev [a,*], M. Dorf [b], S.I. Krasheninnikov [a]

[a] University of California San Diego, La Jolla, CA 92093-0411, USA
[b] Fusion Energy Program, Lawrence Livermore National Laboratory, 7000 EastAvenue L-630, Livermore, CA 94550, USA

ARTICLE INFO

Article history:
Received 15 March 2023
Received in revised form 22 May 2023
Accepted 14 June 2023
Available online 17 June 2023

Keywords:
Collision
Multispecies
Gyrokinetics

ABSTRACT

We implement the multi-species linearized model collision operator, based on the approach proposed by Kolesnikov [1], in the full-f continuum gyrokinetic code COGENT [2]. We describe the operator and use it in several COGENT simulations of highly collisional plasmas. We analyze simulation results with the Braginskii fluid model [3] to illustrate that COGENT recovers both friction and thermal forces. Finally, we simulate the neoclassical transport of heavy impurities with COGENT and illustrate agreement with previously published [4] theoretical results.

1. Introduction

In recent years, various collision operator models have been implemented in numerous gyrokinetic codes in order to simulate Coulomb collisions in tokamak plasmas (see [5–11] and references therein). The correct expression for the Coulomb operator is well known (e.g., Landau form [12]) but often avoided in kinetic modeling because of the high computation cost. Accordingly, only some gyrokinetic codes [13,14] include the correct collision operator, typically referred to as the Fokker-Planck operator. Instead, recent reports [6–11] focus on implementing increasingly complex reduced collision operators and extending these operators for the case of unlike species. The implemented models differ in physical properties, such as, for example, the rate of entropy production and the velocity dependence of the collision frequency. Accordingly, proposed operators have different scope of use. In particular, some recent implementations of unlike collisions (e.g., [9,10]) produce no thermal force which is important for impurity transport in the tokamak edge [15,16].

In this article, we report on implementation of a multi-species linearized collision operator, in the continuum full-f gyrokinetic code COGENT [2]. The operator is based on the Landau operator, and preserves the correct $\lambda \sim (\mathbf{v}_a - \mathbf{v}_b)^4$ dependence of the Coulomb mean free path on a relative velocity $\mathbf{v}_a - \mathbf{v}_b$ of colliding species a and b. This retained velocity dependence enables to recover thermal force, as well as the friction force as they appear in the Braginskii fluid model [3], in the COGENT simulations of highly collisional plasmas. For the case of equal background temperatures of the colliding species, the operator reduces to the operators developed by Sugama [5] and Kolesnikov [1] for delta-f simulations. However, in contrast to the Sugama model, newly implemented operator directly retains collisional thermalization of background Maxwellians with different temperatures, which is consistent with the full-f formulation of the COGENT code. Resulting operator provides a numerically efficient way to simulate collisions between unlike species. It is also worth noting an alternative approach to include energy exchange between background centered Maxwellians implemented in the full-f GYSELA [7] code.

We benchmark this operator in COGENT kinetic simulations of a parallel plasma transport in a slab geometry, against the Braginskii fluid model. We measure values of transport coefficients from kinetic simulations results and find that they are close to values obtained by Braginskii [3] for the Landau operator [12]. Finally, we consider a toroidal annulus geometry and simulate radial impurity transport in the strongly-collisional Pfirsch-Schlüter regime, demonstrating good agreement with the results [4] of the local neoclassical theory.

The paper is organized as follows. Section 2 contains an overview of the COGENT code and describes the newly implemented collision operator. In Section 3, we review COGENT simulations of single component plasma in a slab geometry, and the heavy impurity transport in toroidal geometry. Section 4 summarizes presented results and gives a conclusion.

☆ The review of this paper was arranged by Prof. David W. Walker.

* Corresponding author.
E-mail address: aknyazev@ucsd.edu (A.R. Knyazev).

https://doi.org/10.1016/j.cpc.2023.108829
0010-4655/

2. Model description

This section describes main aspects of the COGENT code and introduces the newly implemented collision model. COGENT is a continuum Eulerian full-f gyrokinetic code. The electrostatic version of the COGENT code (used for simulations in this article) describes coupled evolution of the gyrocenter distribution function and the electrostatic potential for plasma in the external magnetic field. The code solves for a gyrocenter distribution function $f_a(\mathbf{R}_a, v_{||}, \mu_a, t)$ for kinetic species a, where $\mathbf{R}_a$ is the guiding center coordinate, $v_{||} = \mathbf{v}\cdot\mathbf{B}/B$ is the component of velocity $\mathbf{v}$ along the magnetic field $\mathbf{B}$ of magnitude B, and μ_a is the adiabatic invariant of species a with mass m_a. COGENT supports several magnetic $\mathbf{B}$ field geometries: slab, Miller closed-flux model [17] for the core region, and a single-null [18] X-point geometry for cross-separatrix simulations. The numerical algorithm used in COGENT utilizes a high-order finite-volume conservative discretization. Current electrostatic implementation of the code adopts a long wavelength limit $k\rho_i \ll 1$, where ρ_i is the gyroradius of ion species and k is the wavenumber for electrostatic potential variations. For simulations considered in this article, the gyrokinetic full-f equation simulated in COGENT can be written for species a as

$$\frac{\partial B^*_{||a} f_a}{\partial t} + \nabla\cdot(\dot{\mathbf{R}}_a B^*_{||a} f_a) + \frac{\partial}{\partial v_{||}}(\dot{v}_{||} B^*_{||a} f_a) = \\ = B^*_{||a}\left(C(f_a) + C(f_a, f_b)\right), \tag{1}$$

$$\dot{\mathbf{R}}_a = \frac{1}{B^*_{||a}}\left[v_{||}\mathbf{B}^*_a + \frac{1}{e_a}\mathbf{b}\times(e_a\nabla\Phi + \mu_a\nabla B)\right], \tag{2}$$

$$\dot{v}_{||} = -\frac{1}{m_a B^*_{||a}}\mathbf{B}^*_a\cdot(e_a\nabla\Phi + \mu_a\nabla B), \tag{3}$$

$$\mathbf{B}^*_a = \mathbf{B} + \frac{m_a v_{||}}{e_a}\nabla\times\mathbf{b}, \tag{4}$$

where $\mathbf{b} = \mathbf{B}/B$ and $B^*_{||a} = \mathbf{B}_a\cdot\mathbf{b}$, Φ is the long wavelength neoclassical electrostatic potential, $C(f_a)$ is a like-species collision operator, and $C(f_a, f_b)$ is the newly implemented unlike-species collision operator described in the rest of this section. Further implementation details for the axisymmetric (4D) and non-axisymmetric (5D) versions of the COGENT code are available elsewhere [19,20].

The linearized multi-species collision operator presented in this section utilizes the approach described by Kolesnikov in [1]. Specifically, the distribution functions of colliding species f_a and f_b are assumed to be close to Maxwellian distributions with zero bulk velocities,

$$f^M_s = \frac{n_s}{\pi^{3/2} v^3_{Ts}}\exp\left(-\frac{v^2}{v^2_{Ts}}\right);\ s = a, b, \tag{5}$$

where $v = \sqrt{v^2_{||} + 2\mu_s B/m_s}$ is the velocity and $v_{Ts} = \sqrt{2T_s/m_s}$ is the thermal speed of species s with temperature T_s, mass m_s and density n_s. Collision operator $C(f^M_a + \delta f_a, f^M_b + \delta f_b)$ is then approximated with a sum of linear operators as

$$C(f_a, f_b) = C_T(f^M_a, f^M_b) + C_T(\delta f_a, f^M_b) + C_F(f^M_a, \delta f_b). \tag{6}$$

The first two terms in Eq. (6) describe collisions of species a with the Maxwellian background f^M_b of species b. For the background species with charge e_b and mass m_b, the corresponding *test particle* operator C_T can be expressed in the Landau form [12] as

$$C_T(f_a, f^M_b) = -\frac{m_a L^{a/b}}{8\pi}\times \\ \times\frac{\partial}{\partial v_\alpha}\int d\mathbf{v}'\left\{\frac{f_a(\mathbf{v})}{m_b}\frac{\partial f^M_b(\mathbf{v}')}{\partial v'_\beta} - \frac{f^M_b(\mathbf{v}')}{m_a}\frac{\partial f_a(\mathbf{v})}{\partial v_\beta}\right\}U_{\alpha\beta}, \tag{7}$$

$$U_{\alpha\beta} = \frac{1}{u^3}(u^2\delta_{\alpha\beta} - u_\alpha u_\beta);\ u_\beta = v_\beta - v'_\beta, \tag{8}$$

$$L^{a/b} = \ln\Lambda\left(\frac{4\pi e_a e_b}{m_a}\right)^2, \tag{9}$$

where $\ln\Lambda$ is the Coulomb logarithm. This test particle operator C_T can be expressed in COGENT coordinates as a divergence of the probability flux $\mathbf{\Pi}$ in the velocity space,

$$C_T(f_a, f^M_b) = \nabla_v\cdot\mathbf{\Pi} = \frac{\partial\Pi^{v_{||}}}{\partial v_{||}} + \frac{\partial\Pi^{\mu_a}}{\partial\mu_a} = \\ = \frac{\partial}{\partial v_{||}}\left\{\nu_D\left(\frac{\mu_a B}{m_a}\frac{\partial f_a}{\partial v_{||}} - v_{||}\mu_a\frac{\partial f_a}{\partial\mu_a}\right) + \right. \\ \left. + \frac{m_a}{m_a + m_b}\nu_s v_{||} f_a + \nu_{||} v_{||}\left(\mu_a\frac{\partial f_a}{\partial\mu_a} + \frac{v_{||}}{2}\frac{\partial f_a}{\partial v_{||}}\right)\right\} + \\ + \frac{\partial}{\partial\mu_a}\left\{\nu_D\left(\frac{m_a}{B}v^2_{||}\mu_a\frac{\partial f_a}{\partial\mu_a} - v_{||}\mu_a\frac{\partial f_a}{\partial v_{||}}\right) + \right. \\ \left. + \frac{2m_a}{m_a + m_b}\nu_s\mu_a f_a + \nu_{||}\mu_a\left(2\mu_a\frac{\partial f_a}{\partial\mu_a} + v_{||}\frac{\partial f_a}{\partial v_{||}}\right)\right\}. \tag{10}$$

Expression Eq. (10) contains standard notations [21] for deflection frequency ν_D, slow-down rate ν_s and parallel diffusion rate ν_s, given by expressions

$$\nu_D = \nu_{ab}\frac{v^3_{Ta}}{v^3_{Tb}}\left(\frac{\Omega}{\zeta^3} + \frac{1}{\zeta^3}\frac{d\Omega}{d\zeta^2} - \frac{\Omega}{2\zeta^5}\right), \tag{11}$$

$$\nu_s = \nu_{ab}\frac{v_{Ta}}{v_{Tb}}\frac{T_a}{T_b}\left(1 + \frac{m_b}{m_a}\right)\frac{\Omega}{\zeta^3}, \tag{12}$$

$$\nu_{||} = \nu_{ab}\left(\frac{v_{Ta}}{v_{Tb}}\right)^3\frac{\Omega}{\zeta^5}, \tag{13}$$

where $\zeta = v/v_{Tb}$, ν_{ab} is the collision frequency given by

$$\nu_{ab} = \frac{4\pi e^2_a e^2_b\ln\Lambda n_b}{m^2_a v^3_{Ta}}, \tag{14}$$

and Ω is the Maxwell integral [22] that gives normalized value of integrating the Maxwellian distribution over sphere with radius ζ^2,

$$\Omega = \frac{2}{\sqrt{\pi}}\int_0^{\zeta^2}\sqrt{t}e^{-t}dt = \mathrm{erf}(\zeta) - \frac{d\Omega}{d\zeta^2},\ \frac{d\Omega}{d\zeta^2} = \frac{2}{\sqrt{\pi}}\zeta e^{-\zeta^2}.$$

As can be seen from the expression Eq. (10), $C_T(f_a, f^M_b)$ is a differential operator, which makes it cheap to evaluate numerically.

The *field particle* operator $C_F(f^M_a, \delta f_b)$ describes collision of Maxwellian component f^M_a with perturbation δf_b. When written in the Landau form (as done for C_T in Eq. (7)), the field particle operator involves a convolution integral over the velocity space, and is, from the numerical viewpoint, as expensive to evaluate as the full Landau operator. Accordingly, only some codes [23,24] implement the field particle component of the linearized collision operator in the Landau form. Instead, linear collision models typically [5–7] postulate a reduced field particle operator that is more efficient to evaluate numerically. In the collision operator model proposed by Kolesnikov [1], the field particle operator is given by expressions

$$C_F(f_a^M, \delta f_b) = \delta P_{ab}\mathcal{R}_{ab}v_{||} + \delta E_{ab}\mathcal{Q}_{ab}, \tag{15}$$

$$\delta P_{ab} = -\int d\mathbf{v} m_b v_{||} C_T(\delta f_b, f_a^M), \tag{16}$$

$$\delta E_{ab} = -\int d\mathbf{v} \frac{m_b v^2}{2} C_T(\delta f_b, f_a^M), \tag{17}$$

$$\mathcal{R}_{ab}v_{||} = \frac{C_T(m_a v_{||} f_a^M, f_b^M)}{\int d\mathbf{v} m_a v_{||} C_T(m_a v_{||} f_a^M, f_b^M)}, \tag{18}$$

$$\mathcal{Q}_{ab} = \frac{C_T(m_a v^2 f_a^M, f_b^M)}{\int d\mathbf{v}(m_a v^2/2) C_T(m_a v^2 f_a^M, f_b^M)}. \tag{19}$$

Since previous reports [1,25] contain typos in explicit form of the field operator C_F, corrected expressions are given below. In case of equal temperatures $T_a = T_b = T$,

$$\mathcal{R}_{ab} = \frac{3\sqrt{\pi} f_a^M}{4 n_a T}\left(1 + \frac{m_b}{m_a}\right)^{3/2} \frac{\Omega}{\zeta^3}, \tag{20}$$

$$\mathcal{Q}_{ab} = \frac{\sqrt{\pi} f_a^M}{2 n_a T}\left(1 + \frac{m_b}{m_a}\right)^{3/2} \frac{1}{\zeta}\left(\frac{m_a}{m_b}\Omega - \frac{d\Omega}{d\zeta^2}\right). \tag{21}$$

It can be easily demonstrated that C_F provides conservation of momentum,

$$\frac{d}{dt}\int d\mathbf{v} m_a v_{||} f_a = \int d\mathbf{v} m_a v_{||}\Big(C_F(f_a^M, \delta f_b)) + \\ + C_T(\delta f_a, f_b^M) + C_T(f_a^M, f_b^M)\Big) = \delta P_{ab} - \delta P_{ba} - \\ - \int d\mathbf{v} m_b v_{||} C_T(f_b^M, f_a^M) = -\frac{d}{dt}\int d\mathbf{v} m_b v_{||} f_b, \tag{22}$$

and energy (as can be shown analogously to Eq. (22)). From expressions Eqs. (15)-(19), it follows that the field particle C_F operator conserves particles if the test particle operator C_T does. Because of the divergence form Eq. (10) of the test particle operator $C_T(f_a, f_b^M)$, conservation of the particle number density n_a during collisions can be enforced by setting the probability flux to zero $\mathbf{S}\cdot\mathbf{\Pi} = 0$ through the boundaries of the velocity domain S,

$$\int d\mathbf{v} C_T(f_a, f_b^M) = \int_S d\mathbf{S}\cdot\mathbf{\Pi} = 0, \tag{23}$$

where $\mathbf{S}$ is normal to surface S. Since the finite volume discretization scheme used in COGENT exactly recovers the Gauss divergence theorem, the test particle C_T (and, therefore, field particle C_F) operator conserves particles up to machine precision if the probability flux of C_T is adjusted according to Eq. (23).

It is instructive to compare the collision operator given by Eq (6) to previously published [7,8,11] linearized collision operator models. For the case of equal background temperatures, the operator described by Eq. (6) is equivalent to the Sugama collision operator [5]. Accordingly, in thermal equilibrium $T_a = T_b$, the test and field particle operators satisfy adjointness relations

$$\int d\mathbf{v}\frac{\delta f_a}{f_a^M} C_T(\delta g_a, f_b^M) = \int d\mathbf{v}\frac{\delta g_a}{f_a^M} C_T(\delta f_a, f_b^M), \tag{24}$$

$$T_a\int d\mathbf{v}\frac{\delta f_a}{f_a^M} C_F(f_a^M, \delta f_b) = T_b\int d\mathbf{v}\frac{\delta f_b}{f_b^M} C_F(f_b^M, \delta f_a), \tag{25}$$

for arbitrary δg_a, and it was shown (see [5], [26] and references therein) that relations Eq. (24) and Eq. (25) ensure that the operator Eq. (6) satisfies the H-theorem for case of equal temperatures of colliding species. In the case of different background temperatures, $T_a \neq T_b$, the operator given by Eq. (6) is no longer equivalent to the Sugama [5] operator. This is because the latter operator does not include collisions between the Maxwellian backgrounds, and modifies the test particle term in order to ensure that the self-adjointness relation in Eq. (24) holds for unequal temperatures. The Sugama model is suitable for a delta-f [8] formulation, where collisional thermalization between the (fixed) background distribution functions $f_{a,b}^M$ is not included, and, consequently, additional care must be taken to avoid energy transfer from the different-temperature Maxwellian $f_{a,b}^M$ backgrounds into the $\delta f_{a,b}$ perturbations. In contrast to the delta-f approach, the full-f models do not assume fixed background distributions. The energy exchange between background Maxwellians represented by the $C_T(f_a^M, f_b^M)$ term drives the system towards an equilibrium temperature $T = T_a = T_b$. We note that another approach to a linearized collision operator is used in the full-f GYSELA [7,27] code, where a term representing the energy exchange between Maxwellians describes evolution of the background temperatures, and the field particle operator is constructed based on the expansion of a distribution function in spherical harmonics and Laguerre polynomials [7] to recover the friction and thermal forces that will be discussed in Section 3 below.

Finally, we note that the long-wavelength approximation adopted in the model collision operator [Eqs. (6)-(19)] does not account for finite Larmor radius (FLR) effects [8], which, for instance, are required to describe classical transport perpendicular to the magnetic field.

2.1. Stable timestep condition

Time integration in COGENT can be done via explicit fourth-order Runge-Kutta (RK4) or semi-implicit additive Runge-Kutta (ARK) scheme. In this section, we analyze the numerical stability condition for the explicit time stepping scheme, arising from the diffusion in velocity space associated with the test particle operator. We illustrate that diffusion coefficient $D_{\mu\mu}$ along μ grows linearly with velocity v of colliding species a, and this can cause the maximum stable time step δt of the explicit integration scheme to be much less than the collision time $1/\nu_{ab}$.

Because Maxwellian distribution f_b^M is sperically symmetric in the velocity space, the Rosenbluth φ_b, ψ_b potentials associated with the test particle operator are easily found to be

$$\nabla_v^2\varphi_b = f_b^M \Rightarrow \varphi_b = -\frac{n_b}{4\pi v_{Tb}}\frac{1}{\zeta}\left(\Omega + \frac{d\Omega}{d\zeta^2}\right), \tag{26}$$

$$\nabla_v^2\psi_b = \varphi_b \Rightarrow \psi_b = -\frac{n_b v_{Tb}}{8\pi\zeta}\left[(\zeta^2+1)\frac{d\Omega}{d\zeta^2} + \left(\zeta^2 + \frac{1}{2}\right)\Omega\right]. \tag{27}$$

Probability fluxes $\mathbf{\Pi}$ in Eq. (10) can be expressed in drag-diffusion form

$$\Pi^{v_{||}} = A_{v_{||}} f_a + D_{v_{||}\mu}\frac{\partial f_a}{\partial \mu_a} + D_{v_{||}v_{||}}\frac{\partial f_a}{\partial v_{||}}, \tag{28}$$

$$\Pi^{\mu} = A_{\mu} f_a + D_{\mu v_{||}}\frac{\partial f_a}{\partial v_{||}} + D_{\mu\mu}\frac{\partial f_a}{\partial \mu_a}, \tag{29}$$

with the diffusion coefficients given by [14]

$$D_{v_{||}v_{||}} = -L^{a/b}\frac{\partial \psi_b^2}{\partial v_{||}^2} = \frac{1}{2}(\nu_D\frac{2\mu_a B}{m_a} + \nu_{||}v_{||}^2) = \\ = \frac{\nu_{ab} v_{Ta}^3}{2 v_{Tb}}\left(\sin^2(\xi)\left(\frac{1}{\zeta}\frac{d\Omega}{d\zeta^2} + \frac{\Omega}{\zeta} - \frac{\Omega}{2\zeta^2}\right) + \cos^2(\xi)\frac{\Omega}{\zeta^3}\right), \tag{30}$$

$$D_{v_{||}\mu} = -L^{a/b}\frac{2m_a}{B}\mu_a\frac{\partial^2\psi_b}{\partial\mu_a\partial v_{||}} = (\nu_{||}-\nu_D)v_{||}\mu_a = \\ = \nu_{ab}\frac{v_{Ta}^3 m_a}{2B}\sin^2(\xi)\cos(\xi)\left(\frac{3\Omega}{2\zeta^2}-\Omega-\frac{d\Omega}{d\zeta^2}\right), \quad (31)$$

$$D_{\mu\mu} = -L^{a/b}\frac{2m_a^2}{B^2}\mu_a\left(2\mu_a\frac{\partial^2\psi_b}{\partial\mu_a^2}+\frac{\partial\psi_b}{\partial\mu_a}\right) = \\ = \frac{m_a v^4}{8B^2}(\nu_D\sin^2(2\xi)+4\nu_{||}\sin^4(\xi)) = \nu_{ab}\frac{m_a^2 v_{Ta}^3 v_{Tb}}{8B^2}\times \\ \times\left(\sin^2(2\xi)\left(\zeta\Omega+\zeta\frac{d\Omega}{d\zeta^2}-\frac{\Omega}{2\zeta}\right)+4\sin^2(\xi)\frac{\Omega}{\zeta}\right), \quad (32)$$

where $\cos(\xi) = v_{||}/v$. Since $\Omega \to 1$ and $d\Omega/d\zeta^2 \to 0$ for $\zeta \to \infty$, it follows from Eq. (32) that diffusion $D_{\mu\mu}$ grows unbounded with the velocity v of the species a. Recall that explicit schemes typically have a numerical stability threshold d_{FDA}, setting stable resolution criteria $D_{\mu\mu}\delta t/\delta\mu_a^2 < d_{FDA}$. Therefore, stable timestep δt is bounded by condition

$$\nu_{ab}\delta t \lesssim 2d_{FDA}\left(\frac{2B\delta\mu_a}{m_a v_{Ta}^2}\right)^2\frac{v_{Ta}}{v}, \quad (33)$$

where $\delta\mu_a$ is the velocity grid spacing along μ_a. Condition Eq. (33) becomes a severe restriction since, on the one hand, the bulk of the Maxwellian function f_a^M needs to be well resolved in the velocity space $\delta v/v_{Ta} \sim 2B\delta\mu_a/m_a v_{Ta}^2 \sim 10^{-1}$, while, on the other hand, superthermal particles (with velocities $v/v_{Ta} \sim 10$ and above) make important contributions to current and heat flux [28] and need to be retained. Note that, unlike $D_{\mu\mu}$, other diffusion coefficients [given by Eqs. (30) and (31)] are bounded by conditions

$$D_{v_{||}v_{||}} < \frac{\nu_{ab}v_{Ta}^3}{2\sqrt{\pi}v_{Tb}}, \; D_{v_{||}\mu} < \frac{\nu_{ab}v_{Ta}^3 m_a}{3\sqrt{3}B}, \quad (34)$$

and the associated stable timestep conditions are independent of v. Furthermore, recall that the condition in Eq. (33) is derived in the $\zeta = v/v_{Tb} \to \infty$ limit, yet, in practice, the value of ζ is limited by the velocity domain bounds ($|v_{||}|_{max}$ and μ_{max}) of the simulation. Therefore, in general, expressions Eqs. (30)-(32) must be used to determine the stable timestep condition from the diffusion in velocity space.

2.2. Convergence studies

We verify that the operator is implemented correctly by doing a convergence study. We verify that $\mathcal{R}_{ab}$ and $\mathcal{Q}_{ab}$ computed by COGENT from expressions Eqs. (18) and (19) agree with expressions Eqs. (20) and (21). To confirm correct implementation of energy and momentum terms given by Eqs. (16) and (17), we consider an analytically given distribution functions f_a^t (e.g., $f_a^t = (1+0.02v_{||}/v_{Ta}+0.05v_{||}^2/v_{Ta}^2)f_a^M$ used in test shown in Fig. 1), and compare analytical (δP_{ab}^t, δE_{ab}^t) values to COGENT (δP_{ab}^Δ, δE_{ab}^Δ) values from simulation with the same velocity domain boundaries $|v_{||}|_{max}$ and μ_{max}, but with different velocity grid cell sizes $\delta v_{||}$ and $\delta\mu$. In what follows, we label $\delta v_{||}$ and $\delta\mu$ velocity grid sizes as Δ. We repeat COGENT simulation with different resolutions, simultaneously changing $\delta v_{||}$ and $\delta\mu_{||}$ by a factor of two, and measure the residue as shown in Fig. 1 to verify that $|\delta E_{ab}^t - \delta E_{ab}^\Delta| \propto (\Delta/\Delta_0)^2$ and $|\delta P_{ab}^t - \delta P_{ab}^\Delta| \propto (\Delta/\Delta_0)^2$, where Δ_0 is the velocity grid cell size for the COGENT simulation with the velocity resolution $(v_{||}, \mu)$ of 1024×512, as illustrated in Fig. 1. This quadratic rate of convergence is consistent with a second-order cell-centered finite-volume discretization presently utilized for the newly implemented collision operator Eq. (6) in COGENT. We also verified that

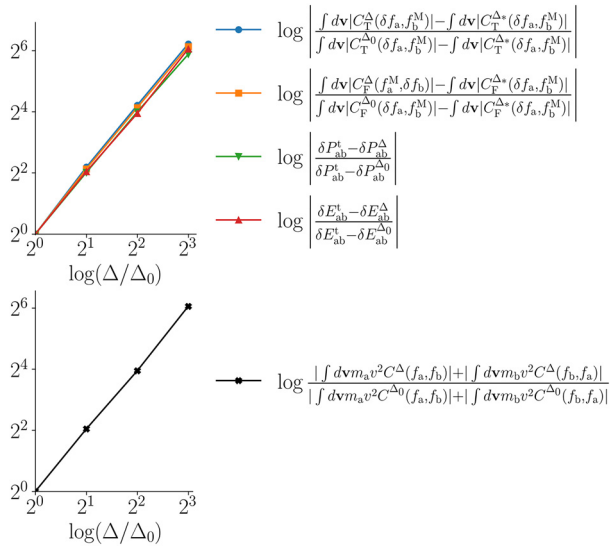

Fig. 1. (Top panel) Example results from the convergence studies, with $f_a = (1+0.02v_{||}/v_{Ta}+0.05v_{||}^2/v_{Ta}^2)f_a^M$, demonstrating quadratic convergence. Grid cells Δ/Δ_0 correspond to $(v_{||}, \mu)$ resolutions 1024×512, 512×256, 256×128, and 128×64, where Δ_0 corresponds to 1024×512. Grid cell size Δ_* corresponds to $(v_{||}, \mu)$ resolution of 2048×1024. All shown simulations have the same velocity domain boundaries μ_{max} and $|v_{||}|_{max}$ given by $2B\mu_{max}/T_a = 27$ and $|v_{||}|_{max}/v_{Ta} = 8$. (Bottom panel) Example results of the energy conservation error in simulations which include collisions between background collisions. The resolution of the velocity domain corresponds to the data on the top panel.

COGENT satisfies both the particle conservation

$$\int d\mathbf{v}C(f_a, f_b) = 0, \quad (35)$$

and the momentum balance

$$\int d\mathbf{v}m_a v_{||}C(f_a, f_b) + \int d\mathbf{v}m_b v_{||}C(f_b, f_a) = 0, \quad (36)$$

up to numerical precision, regardless of the velocity domain resolution. The particle conservation Eq. (35) is obtained by setting the probability flux through the $|v_{||}|_{max}$ and μ_{max} boundaries to zero, as in Eq. (23).

The energy conservation

$$\int d\mathbf{v}\frac{m_a v^2}{2}C(f_a, f_b) + \int d\mathbf{v}\frac{m_b v^2}{2}C(f_b, f_a) = 0 \quad (37)$$

is demonstrated in the bottom panel of Fig. (1) as a function of the velocity grid resolution. Note that the error in energy conservation comes entirely from the terms describing the background Maxwellian interactions, i.e., $C_T(f_a^M, f_b^M)$ and $C_T(f_b^M, f_a^M)$. When background Maxwellians are in the thermal equilibrium, the corresponding collision term vanishes $C_T(f_a^M, f_b^M) = 0$ and can be excluded from the operator, resulting in energy conservation up to machine precision for all velocity resolutions.

Recall that the denominators of the $\mathcal{R}_{ab}$ and $\mathcal{Q}_{ab}$ terms of the field operator in Eqs. (18) and (19) are designed to balance momentum and energy loss caused by the test particle operator for species b, as illustrated in Eq. (22). To recover the corresponding discretized energy and momentum conservation properties (Eqs. (36), (37)) up to numerical precision, we employ numerical evaluation and integration of the denominators in expressions Eqs. (18) and (19), instead of evaluating them analytically as in Eq. (20) and (21).

3. COGENT simulations in the highly collisional regime

In this section, we use the model collision operator to simulate transport in case of high mass ratio $m_b \gg m_a$ and for high enough

collisionality to assume small deviations from a Maxwellian distribution for colliding species a and b, justifying the use of a linearized collision operator. Collisions in such regime produce thermal and friction forces, as was demonstrated by Braginskii [3] for electron-ion plasma. In what follows, background Maxwellian distributions are fixed and have equal temperature $T_a = T_b = T$, so $C_T(f_a^M, f_b^M) = 0$.

The friction force along the magnetic field, resulting from operator Eq. (6), can be expressed as

$$\int d\mathbf{v} m_a v_{||} C(f_a, f_b) = \delta P_{ab} - \delta P_{ba}, \tag{38}$$

with δP_{ab} and δP_{ba} defined by Eq. (16).

Our first goal is to verify that, in linear approximation, the friction force Eq. (38) from the model operator agrees with the result from Braginskii's [3] original work. We consider the bulk velocities of electrons u_a and ions u_b (relative to the velocity of background Maxwellians f_s^M) to be much less than their thermal speeds v_s. We follow Braginskii's approach and compute the friction force on light species by approximating the distribution function to first order as

$$f_a \approx f_a^M \left(1 + \frac{2\mathbf{u}_a \mathbf{v}}{v_a}\right). \tag{39}$$

Since for the test particle collision operator the energy transfer rate between the light species a and the heavy species b is a factor of m_a/m_b smaller than the momentum transfer rate, we can calculate the δP_{ba} as

$$\begin{aligned} \delta P_{ba} &= \int d\mathbf{v} \frac{m_a v_{||} n_b L^{a/b}}{8\pi} \frac{\partial}{\partial v_\alpha} \frac{v^2 \delta_{\alpha\beta} - v_\alpha v_\beta}{v^3} \frac{\partial \delta f_a}{\partial v_\beta} = \\ &= \frac{n_b m_a L^{a/b}}{2\pi} \int d\mathbf{v} \frac{v_{||}}{v^3} \frac{u_{a\beta} v_\beta}{v_{Ta}^2} f_a^M = \frac{4\nu_{ab} m_a n_a}{3\sqrt{\pi}} u_a. \end{aligned} \tag{40}$$

The δP_{ba} obtained in Eq. (40) depends on the u_a, yet it is clear from the physics of the Coulomb collisions that the friction force must depend on the relative bulk velocity $u_a - u_b$. Therefore, the contribution from δP_{ab} must also be considered. To calculate δP_{ab}, we use the Landau form of the test particle operator given by Eq. (7) in the expression Eq. (16), and expand the relative velocity tensor defined in Eq. (8) to first order as

$$U_{\alpha\beta} \approx \frac{v'^2 \delta_{\alpha\beta} - v'_\alpha v'_\beta}{v'^3} + v_\gamma \frac{\partial}{\partial v'_\gamma} \left(\frac{v'^2 \delta_{\alpha\beta} - v'_\alpha v'_\beta}{v'^3} \right), \tag{41}$$

with the ratio between the velocities of species b and a as the expansion parameter. Combining Eqs. (7), (16) and (41), we can evaluate δP_{ab} as

$$\begin{aligned} \delta P_{ab} &= \int d\mathbf{v} m_b v_{||} \frac{m_b L^{b/a}}{8\pi} \frac{\partial}{\partial v_\alpha} \int d\mathbf{v}' \frac{\delta f_b(\mathbf{v})}{m_a} \frac{\partial f_a^M(\mathbf{v}')}{\partial v'_\beta} \\ &\quad \times \left\{ \frac{v'^2 \delta_{\alpha\beta} - v'_\alpha v'_\beta}{v'^3} + v_\gamma \frac{\partial}{\partial v'_\gamma} \left(\frac{v'^2 \delta_{\alpha\beta} - v'_\alpha v'_\beta}{v'^3} \right) \right\} \\ &= -\frac{m_b^2 L^{b/a}}{8\pi m_a} \int d\mathbf{v} \delta f_b v_{||} \int d\mathbf{v}' \frac{v'^2 \delta_{\alpha\beta} - v'_\alpha v'_\beta}{v'^3} \frac{\partial f_a^M}{\partial v'_\beta \partial v'_{||}} \\ &= \frac{4}{3\sqrt{\pi}} \nu_{ba} \sqrt{\frac{m_a}{m_b}} m_b n_b u_b, \end{aligned} \tag{42}$$

where

$$u_b = \frac{1}{n_b} \int d\mathbf{v} \delta f_b v_{||}. \tag{43}$$

Combining expressions Eq. (40) and Eq. (42) above, we find that the linear approximation for friction force

$$\begin{aligned} &\int d\mathbf{v} m_a v_{||} C(f_a, f_b) = \delta P_{ab} - \delta P_{ba} = \\ &= \frac{4\nu_{ab} m_a n_a}{3\sqrt{\pi}} (u_b - u_a) = -\int d\mathbf{v} m_b v_{||} C(f_b, f_a). \end{aligned} \tag{44}$$

matches the result of Braginskii. This is to be expected, since, in the infinite mass ratio $m_b/m_a \to \infty$ limit, the operator described by Eq. (6) is the same as the Landau operator. Indeed, the test particle $C_T(\delta f_a, f_b^M)$ operator in this limit reduces to the Lorentz operator, while the field particle operator vanishes for infinitely heavy species b.

3.1. Modeling electric conductivity with COGENT

We now simulate the friction force in COGENT with the setup described in this paragraph. For simplicity, we consider a slab geometry with two species (a and b), which are initialized with uniform Maxwellian distributions f_a^M and f_b^M, respectively. We set masses of colliding species to $m_a = m_p$, $m_b = 100 m_p$ in the units of proton mass m_p. The charge of species a is set equal to the electron charge, $e_a = -|e|$. The charge of the heavy species $e_b = Z_b|e|$ is varied between simulations. The density n_a of species a is set to $10^{21}\ m^{-3}$, and the density n_b of species b is set by the quasi-neutrality condition

$$e_a n_a + e_b n_b = 0. \tag{45}$$

The temperature of both species is homogeneous and set to 20 eV. We consider a slab geometry with a uniform fixed magnetic $B\mathbf{e}_z$ and electric $E\mathbf{e}_z$ fields along the z-axis, and periodic boundary conditions in the z-direction. For the outlined simulation setup, the kinetic equation (1) solved in COGENT for the species a reduces to

$$\frac{\partial f_a}{\partial t} + \frac{e_a E}{m_a} \frac{\partial f_a}{\partial v_{||}} = C(f_a) + C(f_a, f_b). \tag{46}$$

Collisions $C(f_a, f_b)$ between species a and species b are modeled using the operator described in Section 2. Note that, for a finite charge e_b of species b, the impact of collisions $C(f_a)$ between light species a on their distribution function f_a is compatible to the impact of the collisions between species a and b, $C(f_a, f_b) \sim C(f_a)$. Therefore, collisions between species a must be included into the simulation with finite charge state of species b, $Z_b \sim 1$. Various like-species collision models are available [29] in the COGENT code, including the full Fokker-Planck [14] collision operator $C_{FP}(f_a)$, and a model collision operator $C_A(f_a)$ proposed by Abel [30] that is similar to the operator $C(f_a, f_b)$ described in Section 2 (both $C_A(f_a)$ and $C(f_a, f_b)$ are based on the linearized Landau collision operator). As we mentioned earlier, the Fokker-Planck operator gives the highest fidelity, but is expensive to evaluate numerically since it requires solving a pair of Poisson equations [14] for the Rosenbluth potentials. Therefore, it is of interest to assess the impact of replacing the Fokker-Planck operator $C_{FP}(f_a)$ with the Abel collision operator $C_A(f_a)$, which is much faster to evaluate. The use of a linearized collision model in the considered simulations can be justified for the case where the magnitude of the electric field E is much less than the Dreicer [31] field E_D. Because the role of electrons is assumed here by the species a with a mass of a proton, the corresponding Dreicer field is $E_D \sim$ 1 kV/m. For $E \ll E_D$ and homogeneous background profiles, the deviations from the Maxwellian can be assumed to be small and the use of linearized collision operators is justified. In what follows, we perform two sets of COGENT simulations, where the like-species collisions of the light species a are described with

either the Fokker-Planck, $C_{\rm FP}$, or the model Abel operator, $C_{\rm A}$. In addition to verification purposes, this test elucidates validity limits of the reduced Abel operator.

We simulate the described setup in COGENT over hundred collision times $1/\nu_{\rm ab}$, allowing the bulk velocities

$$u_{\rm b} \equiv \frac{1}{n_{\rm b}} \int d\mathbf{v} v_{||} \delta f_{\rm b} = -\frac{Z_{\rm b} m_{\rm a}}{Z_{\rm a} m_{\rm b}} u_{\rm a}, \tag{47}$$

$$u_{\rm a} \equiv \frac{1}{n_{\rm a}} \int d\mathbf{v} v_{||} \delta f_{\rm a}, \tag{48}$$

to reach a steady state. Note that the right equality in Eq. (47) follows from the quasi-neutrality condition Eq. (45) and momentum conservation Eq. (36). We then analyze the kinetic simulation results with the Braginskii [3] fluid model,

$$m_{\rm s} n_{\rm s} \frac{du_{\rm s}}{dt} + \frac{\partial P_{\rm s}}{\partial z} = e_{\rm s} n_{\rm s} E + R_{\rm s}, \tag{49}$$

$$\frac{3}{2} n_{\rm s} \frac{dT_{\rm s}}{dt} + P_{\rm s} \frac{\partial u_{\rm s}}{\partial z} = -\frac{\partial q_{\rm s}}{\partial z} + Q_{\rm s}, \tag{50}$$

where $P_{\rm s} = n_{\rm s} T_{\rm s}$ is the pressure, $Q_{\rm s}$ is the heat from friction given for species a as

$$Q_{\rm a} = \int d\mathbf{v} \frac{m_{\rm a} v^2}{2} C(f_{\rm a}, f_{\rm b}), \tag{51}$$

$R_{\rm s} = R_{\rm u,s} + R_{\rm T,s}$ is the parallel force combined from friction $R_{\rm u,s}$ and thermal $R_{\rm T,s}$ forces expressed for species a as

$$\begin{aligned} R_{\rm a} &= \int \mathbf{d} v m_{\rm a} u_{||} C(f_{\rm a}, f_{\rm b}) = R_{\rm u,a} + R_{\rm T,a} = \\ &= -C_1 \frac{4\nu_{\rm ab} m_{\rm a} n_{\rm a}}{3\sqrt{\pi}} (u_{\rm a} - u_{\rm b}) - C_2 n_{\rm a} \nabla_{||} T_{\rm a}, \end{aligned} \tag{52}$$

and $q_{\rm s}$ is the parallel heat flux expressed for species a as

$$\begin{aligned} q_{\rm a} &= \int d\mathbf{v} \frac{m_{\rm a}}{2} (\mathbf{v} - u_{\rm a}\mathbf{e}_z)^2 (v_{||} - u_{\rm a}) f_{\rm a} = q_{\rm u,a} + q_{\rm T,a} = \\ &= C_2 n_{\rm a} T_{\rm a} (u_{\rm a} - u_{\rm b}) - C_3 \frac{3\sqrt{\pi} n_{\rm a} T_{\rm a}}{4 m_{\rm a} \nu_{\rm ab}} \nabla_{||} T_{\rm a}. \end{aligned} \tag{53}$$

The transport coefficients C_1, C_2, C_3 depend on details of a collision model and can be inferred from the results of COGENT simulation. It is important to emphasize that the thermal force $R_{\rm T,a}$ arises from the velocity dependence of the Coulomb collisions $\lambda \sim (\mathbf{v}_{\rm a} - \mathbf{v}_{\rm b})^4$, and the unlike-species collision operator must recover this dependence in order to recover the thermal force in Eq. (52). For example, the thermal force $R_{\rm T,a}$ in Eq. (52) cannot be recovered from Bhatnagar-Gross-Krook (BGK) [32] collision operator $C_{\rm BGK}(f) = \nu(f - f^{\rm M})$ with ν independent of a particle velocity. Indeed, the force produced by BGK operator is

$$\int \mathbf{v} C_{\rm BGK}(f) d\mathbf{v} = \nu \left(\int \mathbf{v} f d\mathbf{v} - \int \mathbf{v} f^{\rm M} d\mathbf{v} \right), \tag{54}$$

which only depends on the bulk velocities of distributions f and $f^{\rm M}$ and does not depend on temperature gradients. Likewise, the thermal force $R_{\rm T,a}$ is not recovered by the Lenard-Bernstein-Dougherty (LBD) [33,34] operator of the form

$$C_{\rm LBD}(f_{\rm a}) = L \frac{\partial}{\partial v_\alpha} \left[(\mathbf{v} - \mathbf{V}^{\rm LBD}) f_{\rm a} + D^{\rm LBD}_{\alpha\beta} \frac{\partial f_{\rm a}}{\partial v_\beta} \right], \tag{55}$$

where L, $V^{\rm LBD}$ and $D^{\rm LBD}$ are some functions independent of velocity, as in, for example, recently reported GKeyll [9] or GENE-X [10] implementations. Indeed, the force from the $C_{\rm LBD}$ collision operator described in Eq. (55) is

$$\int \mathbf{v} C_{\rm LBD}(f_{\rm a}) d\mathbf{v} = -L \left(\int \mathbf{v} f_{\rm a} d\mathbf{v} - \mathbf{V}^{\rm LBD} \right), \tag{56}$$

and in order for this expression to recover the thermal force $R_{\rm T,a}$ from expression (52) would require for the $\mathbf{V}^{\rm LBD}$ function to have a particular explicit $\nabla_{||} T$ dependence. Current LBD implementations often [9,10] disregard the thermal force entirely, despite this force being important [16] for the impurity transport.

The multi-species collision operator given by Eq. (6) is based on the test particle operator $C_{\rm T}$ which preserves the velocity dependence of Coulomb collisions, and therefore can recover the thermal force. For simulations described in Sections 3.1 and 3.2, we measure the parallel force $R_{\rm a}$ and the heat flux $q_{\rm a}$, verify that they have the forms given by Eq. (52) and Eq. (53), and compute the transport coefficients $C_{1,2,3}$.

For the simulation setup with a fixed electric field described above, a steady-state solution corresponds to a balance between the parallel force $R_{\rm a}$ and the electric force $e_{\rm a} n_{\rm a} E$ [see Eqs. (49) and (52)], giving

$$C_1 = \frac{3\sqrt{\pi} |e_{\rm a}| E}{4\nu_{\rm ab} m_{\rm a} n_{\rm a} |u_{\rm a} - u_{\rm b}|}. \tag{57}$$

From simulation without a-a collisions, we obtain $C_1 = 0.30$ from Eq. (57). This value is very close to the value $C_1^{\rm B} = 0.29$ reported by Braginskii for the case of an electron-ion plasma with $Z_{\rm b} \to \infty$. Such agreement is expected since $Z_{\rm b} = e_{\rm b}/|e| \to \infty$ allows to neglect electron-electron collisions in the electron-ion problem, and electrons correspond to the species a in the described simulation. For finite $Z_{\rm b}$, collisions between the light species a must also be included in the corresponding COGENT simulation. We use Eq. (57) to measure the transport coefficient in COGENT simulations with various values of $e_{\rm b}$ and compare them to the corresponding results from the Braginskii's problem for an electron-ion plasma [3,4], as shown in the top and bottom left panel in Fig. 2. We also perform several additional runs with different values of the electric field, E, to verify that the measured force is proportional to $u_{\rm a} - u_{\rm b}$, in agreement with the expression for the friction force $R_{\rm u,a}$ in Eq. (52). These runs are illustrated in the bottom right panel in Fig. 2. When the Fokker-Planck operator $C_{\rm FP}(f_{\rm a})$ is used to model collisions between the species a, the values of C_1 are within $3-6\%$ of Braginskii's results for all $Z_{\rm b}$. Recall that the difference between the newly implemented operator Eq. (6) and the linearized Landau operator vanishes in the limit of high mass ratios, justifying the observed agreement with Braginskii's results for the electron ion plasma since $m_{\rm e} \ll m_{\rm i}$. Furthermore, in simulations where the Abel collision operators $C_{\rm A}(f_{\rm a})$ are used instead of the Fokker-Planck $C_{\rm FP}(f_{\rm a})$ operator, the values of C_1 are within 20% of Braginskii's results. When using the model collision operator $C_{\rm A}(f_{\rm a})$ for the like-species collisions, the difference with the values reported by Braginskii is the largest for the smallest charge of species b, $Z_{\rm b} = 1$, which is to be expected since, for higher charge state $Z_{\rm b}$, the influence of like-species collisions on the light species distribution function $f_{\rm a}$ decreases relative to the influence of collisions between the light species a and the heavy species b.

3.2. Thermal force and heat flux coefficients measurement with COGENT

The heat flux $q_{\rm a}$ for species a is given by Eq. (53) in the Braginskii model presented above. We use Eq. (53) to measure C_2 in the simulation setup from Section 3.1 as

$$C_2 = \frac{q_{\rm a}}{n_{\rm a} T (u_{\rm a} - u_{\rm b})}, \tag{58}$$

and present results in Fig. 2. For the simulation corresponding to $Z_{\rm b} \to \infty$ (i.e., without self-collisions of species a), Eq. (58) gives $C_2 = 1.44$, which is close to the heat flux coefficient value

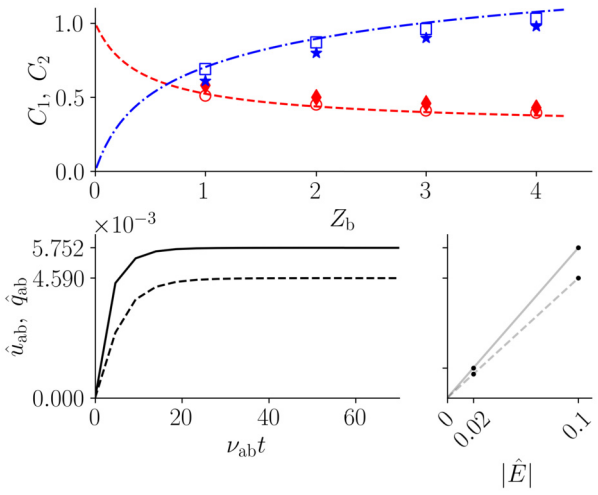

Fig. 2. (Top panel): Values of transport coefficients C_1 (red circle and diamond labels) and C_2 (blue square and star labels) from COGENT simulation of the setup described in Section 3.1, measured using Eq. (57) and Eq. (58) for various e_b. The red dashed line and blue dash-dot line show Braginskii's values [3,4] for electron-ion transport coefficients C_1 and C_2, respectively. For simulations with Abel collision operator $C_A(f_a)$ for collisions between species a, the transport coefficients C_1 (diamonds) and C_2 (stars) are within 20% of the Braginskii's values. When Fokker-Planck operator is used to model a-a collisions, agreement of C_1 (circles) and C_2 (squares) with Braginskii is within $3-6\%$. (Bottom left panel): Time series of the bulk velocity u_a (solid line) and heat flux (dashed line) q_a for simulation with $e_b = 2|e|$, illustrating the steady state. (Bottom right panel) Scaling of steady state velocity (top line) and heat flux (bottom line) from COGENT simulations with different E, demonstrating that steady state bulk velocity and heat flux scale linearly with E, in agreement with theory. Velocity is normalized by v_{Ta}, heat flux by $n_a T_a v_{Ta}$, distance by $\tilde{l} = 1$ m and electric field by $T_a/(|e|\tilde{l})$. The simulation has velocity domain boundaries $|v_{||}|_{max}/v_{Ta} = 8$, $\mu_{max}B/T_a = 12$, and velocity grid resolution $n_{v_{||}} = n_\mu = 128$. (For interpretation of the colors in the figure(s), the reader is referred to the web version of this article.)

of $C_2^B = 1.5$ reported by Braginskii for the electron-ion problem. For the simulations corresponding to finite Z_b, the values of C_2 are within 3-6% of Braginskii's results in simulations where the Fokker-Planck operator $C_{FP}(f_a)$ is used to simulate collisions between the light species a, as shown in Fig. 2. When the Fokker-Planck operator is replaced by the Abel linearized collision operator $C_A(f_a)$, the observed C_2 values are within 20% of Braginskii's results.

Our next goal is to consider a hydrodynamic equilibrium in the presence of the temperature gradient along the magnetic field, to measure the thermal $R_{T,a}$ force in Eq. (52) and the $q_{T,a}$ component of the parallel thermal flux in Eq. (53). We do this in the rest of this section.

We consider a slab geometry introduced in Sec. 3.1, although we turn off the electric field. For the outlined simulation setup, the kinetic equation (1) solved by COGENT for the species a can then be simplified to

$$\frac{\partial f}{\partial t} + \frac{\partial}{\partial z}(v_{||} f_a) = C(f_a) + C(f_a, f_b), \tag{59}$$

where z is the coordinate along the magnetic field. We set the initial temperature profile for both species as

$$\frac{T_s}{T_{s,0}} = 1.05 - 0.05\left(1 + \exp\left(2\pi \frac{z - z_{min}}{z_{max} - z_{min}} - \pi\right)\right)^{-1} \tag{60}$$

where $T_{s,0} = 20$ eV, $z_{min} = 0$ m and $z_{max} = 2$ m. The density profile for each species is set to $n_{s,0}T_{s,0}/T_s$ so that the system is in hydrodynamic equilibrium $\nabla p_s = 0$. We take $n_{a,0} = 5 \times 10^{21}$ m^{-3} and $n_{b,0}$ is set by the quasi-neutrality condition given by Eq. (45). The masses of species are set to $m_a = m_p$ and $m_b = 100 m_p$ as in the setup from the previous section, $e_a = -|e|$, and the value of e_b is

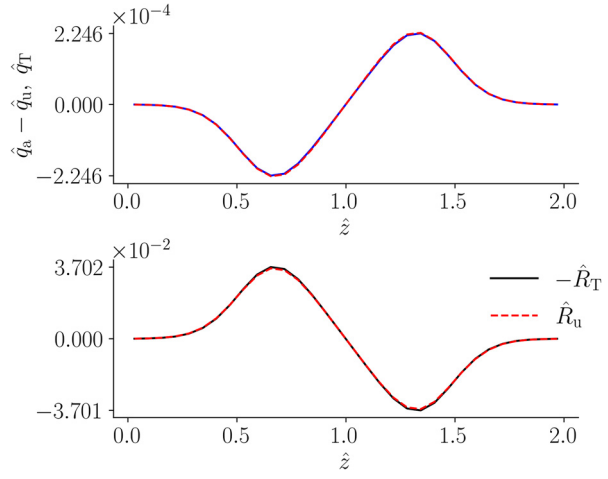

Fig. 3. (Top panel): Profiles of the thermal heat flux $q_{T,a}$ and residue $\mathbf{q}_a - \mathbf{q}_u$, as defined in Eq. (53). (Bottom panel) profiles of the pressures from friction R_u and thermal R_T forces at steady state, demonstrating $|u_a - u_b| \propto \nabla_{||} T$ in agreement with Eq. (52). Velocity is normalized by v_{Ta}, heat flux by $n_{a,0}T_a v_{Ta}$, distance by $\tilde{l} = 1$ m, pressure by $n_{a,0}m_a v_{Ta}^2/\tilde{l}$. Simulated velocity grid is bounded by $|v_{||}|_{max}/v_{Ta} = 8$, $\mu_{max}B/T_a = 12$ and has resolution $n_{v_{||}} = n_\mu = 128$. Domain resolution along the magnetic field is $n_z = 32$.

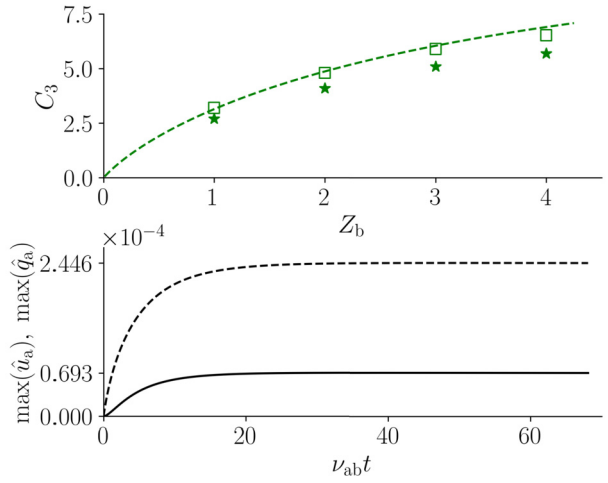

Fig. 4. (Top panel): Values of the conductive heat flux coefficient C_3 (green labels) from COGENT simulation of the setup described in Section 3.2, measured using Eq. (53) for various e_b. The green dashed line shows heat flux coefficient C_3 reported by Braginskii [3,4]. Simulations with Abel like-species collision operator $C_A(f_a)$ are labeled with stars and agree within 20% of the Braginskii values. When the Fokker-Planck C_{FP} operator is used instead to model the like-species collisions, the agreement of C_3 values (marked with square labels) with Braginskii's results is improved to within $3-6\%$. (Bottom panel) Time series of relative velocity $\hat{u} = |\hat{u}_a - \hat{u}_b|$ (solid lines), and heat flux $\hat{q}_a$ (dashed lines) from simulation with $e_b = 3|e|$, illustrating the steady state. Velocity is normalized by v_{Ta}, heat flux by $n_{a,0}T_a v_{Ta}$.

varied between the simulations. COGENT simulations demonstrate that the bulk velocities and heat fluxes reach their quasi-stationary state values after about a dozen of collisional times. In this quasi-stationary state, the thermal force, $R_{T,a}$, should be balanced by the friction force, $R_{u,a}$, according to Eqs. (49) and (52). This property is confirmed in our simulations, as illustrated in Fig. 3 and bottom panel of Fig. 4. From Eq. (52) and $R_{u,a} + R_{T,a} = 0$, we can measure the C_1/C_2 ratio. For example, for $Z_b = 3$, in the simulation with the Abel collision operator C_A, we recover the ratio $C_2/C_1 = 1.92$. Recall that we previously measured $C_1 = 0.46$ and $C_2 = 0.9$ for the case of $Z_b = 3$ in the counterpart simulation which included external electric field (see Sec. 3.1). For that case, we obtained the transport coefficients from the steady-state values of the friction

force (C_1) and the heat flux (C_2). It is instructive to note that the ratio of those coefficients $C_2/C_1 = 1.96$ is within 2% from what we obtain here from the force balance. This illustrates the Onsager symmetry of the transport coefficients. The Onsager principle follows from $(t, B) \to (-t, -B)$ invariance of underlying equations of motion and yields the transport coefficient for the convective heat flux [the first term in the right-hand side of Eq. (53)] to be the negative of the transport coefficient for the friction force [the second term in the right-hand-side of Eq. (52)]. This principle is represented in the self-adjointness relations Eqs. (24) and (25) of the collision operator (see [26] and references therein). Note that the Onsager symmetry is related to the entropy production [26] rate. Therefore, model operators which do not recover Onsager symmetry do not, in general, result in the correct rate of entropy production, which can be important [35] for kinetic studies. The model operator in Eq. (6) does recover Onsager symmetry for the case $T_a = T_b$ considered here, and we verify that the C_2/C_1 ratio measured from the two different setups described in Secs. 3.1 and 3.2 agree within 2% for all Z_b we simulated. We can therefore use the value of C_2 obtained from Eq. (58) to measure the transport coefficient C_3 in the Eq. (48) as illustrated in the top panel of Fig. 3. Without the like-species collisions for species a, we obtain $C_3 = 12.4$, which recovers Braginskii's value $C_3^B = 12.5$ for the $Z_b \to \infty$ case in the electron-ion problem. Similarly to previous results, when we use the Fokker-Planck operator $C_{FP}(f_a)$ to simulate collisions between the light species a, the values of the conductive heat flux coefficient C_3 from COGENT simulations are within $3-6\%$ of Braginskii's result for all Z_b, as illustrated in the top panel of Fig. 4. In the corresponding simulations with the Abel collision operator $C_A(f_a)$, we obtain C_3 values within 20% of Braginskii's result.

In summary, in this section we performed simulations using COGENT with the model collision operator given by expression Eq. (6) to measure the parallel transport coefficients $C_{1,2,3}$ in a strongly collisional regime for a two-component plasma with a large species mass ratio $m_a/m_b = 1/100$. For the case where the Fokker-Planck operator $C_{FP}(f_a)$ is used to model the like-species collisions for the light species a, the results of the COGENT simulations for all transport coefficients are found to be in good agreement (within 3-6%) with Braginskii's results for an electron-ion plasma. For the case where the linearized Abel operator $C_A(f_a)$ is used to model a-a collisions, the departure from Braginskii's results increases to 20%. The maximum difference is observed for smaller values of Z_b, consistent with a pronounced role of the like-species collisions for $Z_b \sim 1$. We also verified that the Onsager symmetry relationship is recovered in our simulations for the case of equal $T_a = T_b$, as expected from the self-adjointness of the model unlike collision operator.

It is expected that the model unlike-species collision operator given by Eq. (6) does not, in general, yield physically accurate transport coefficient outside the high mass ratio limit addressed in this section, since the error from the ad-hoc field particle operator is significant for $m_a \sim m_b$. This limitation can be addressed by utilizing the moment method [36] to further improve a linearized collision model as proposed by Sugama in Ref. [6].

3.3. Modeling radial neoclassical transport in the presence of heavy impurities with COGENT

In this section, we consider a plasma of electrons, ions, and heavy impurities in a concentric circular tokamak geometry. The magnetic field geometry is given by

$$B_{\phi,\theta}(r,\theta) = \frac{B_{T,p} R_0}{R_0 + r\cos(\theta)}, \tag{61}$$

where r is the minor radius coordinate, θ is the poloidal angle, B_T and B_p are the toroidal and poloidal components of the magnetic field. We take the major radius of the tokamak to be $R_0 = 8.5$ m. The minor radius coordinate ranges from $r_{min} = 0.8075$ m to $r_{max} = 0.8925$ m, so the middle of the simulation domain is located at $r_0 = (r_{min} + r_{max})/2 = 0.85$ m and the tokamak aspect ratio is $\epsilon = r_0/R_0 = 0.1$ We consider plasma transport in a Pfirsch-Schlüter regime, i.e., for collisionality

$$\nu^* = \frac{\nu_{ab}\epsilon^{-3/2} q R_0}{v_{Tb}} \gg 1, \tag{62}$$

where $q \sim \epsilon B_T/B_p \sim 1.14$ is the characteristic safety factor, ν_{ab} is the collision frequency defined in Eq. (14), main plasma ions are denoted as species a with mass $m_a = m_p$ and charge $e_a = |e|$, and impurities are denoted as species b with $m_b = 100 m_p$ and charge $e_b = 2|e|$. We simulate a strongly magnetized plasma by taking $B_T = 28.9$ T, $B_p = 2.53$ T, and assuming the background temperature $T = 500$ eV for all species. Initial condition for f_a and f_b correspond to a local Maxwellian distribution function with uniform temperature and density profiles given by

$$n_s = n_{s,0}\left(1 - 0.05\tanh\left(2\pi\frac{r - r_{min}}{r_{max} - r_{min}} - \pi\right)\right), \tag{63}$$

where $n_{a,0} = 2.8 \times 10^{20}$ m^{-3} and $n_{b,0} = 7 \times 10^{19}$ m^{-3}. These plasma parameters correspond to $\nu^* \approx 34 \gg 1$. For the outlined parameters, plasma is strongly magnetized, with the gyroradius much smaller than the mean free path $\rho_a \ll \lambda_a$.

The electron density is described by the linear Boltzmann response as

$$n_e = \langle n_a + Z_b n_b\rangle\left(1 + \frac{e\Phi}{T} - \frac{e\langle\Phi\rangle}{T}\right), \tag{64}$$

where the angular brackets represent the flux surface average

$$\langle f\rangle = \oint f\frac{dl_\theta}{B_\theta}\Big/\oint\frac{dl_\theta}{B_\theta}. \tag{65}$$

In contrast to the slab geometry simulations presented in Secs. 3.1 and 3.2, here we also evolve the electric field. This is done in COGENT by including the gyrokinetic Poisson equation [29,37] in the long-wavelength limit

$$\sum_s \frac{4\pi e_s^2}{m_s\Omega_s^2}\nabla_\perp\cdot(n_s^{gc}\nabla_\perp\Phi) = 4\pi e\left(n_e - \sum_s n_s^{gc}\right), \tag{66}$$

where $\Omega_s = e_s B/m_s c$ is the gyrofrequency, n_s^{gc} is the gyrocenter density given by

$$n_s^{gc} = \frac{2\pi}{m_s}\int B_{||s}^* f_s dv_{||} d\mu_s, \tag{67}$$

and $\nabla_\perp = \nabla - \mathbf{b}(\mathbf{b}\cdot\nabla)$. The radial boundary conditions for the Poisson equation (66) is

$$\left\langle\sum_s \frac{c^2 n_s m_s}{B^2}|\nabla\psi|^2\right\rangle\frac{\partial\Phi}{\partial\psi} = \int_0^t dt\langle\nabla\psi\cdot\sum_s \mathbf{j}_s\rangle, \tag{68}$$

where ψ denotes the flux surface and $\mathbf{j}_s$ is the gyrocenter current density given by

$$\mathbf{j}_s = \frac{2\pi e_s}{m_s}\int \dot{\mathbf{R}}_s f_s B_{||}^* dv_{||} d\mu_s. \tag{69}$$

We solve Eq. (66) with Neumann radial boundary conditions together with the gyrokinetic equation (1) in the annular toroidal

geometry. We run simulation for about $100/\nu_{ab}$ to allow for collisional GAM [38] relaxation and the establishment of steady radial profiles for radial particle fluxes. We analyze simulation results by using the analogy [4] between electron-ion and proton-heavy impurity transport problems. In the ion-heavy impurity problem, the protons (species a) play the role of "electrons", while the impurities (species b) play the role of "protons" in the Braginskii treatment. In the electron-ion problem, the electron-electron collision operators scale as n_e and electron-ion collision operator scale as $n_i Z^2$. In the ion-impurity problem considered here, ion-ion collision operators scale as n_a and the ion-impurity collision operator scales as $n_b Z_b^2$. This suggests [4] that the ion-heavy impurity transport problem is analogous to the electron ion problem of Braginskii for the case of the ion charge Z_b given by $\alpha = n_b e_b^2/(n_a e_a^2)$. In the high aspect ratio $\epsilon = r/R \ll 1$ toroidal geometry, it was shown [4] that the radial magnetic surface averaged particle $\langle \Gamma_a \cdot \nabla r\rangle$ flux can be expressed in terms of the parallel transport coefficients C_1, C_2 and C_3 from Eqs. (52)-(53) as

$$\langle \Gamma_a \cdot \nabla r\rangle = -2q^2 D_a n_a \left(\left(C_1 + \frac{C_2^2}{C_3}\right)\times \right.$$
$$\left. \times \left(\frac{\partial \ln p_a}{\partial r} - \frac{T_b}{Z_b T_a}\frac{\partial \ln p_a}{\partial r}\right) - \frac{5}{2}\frac{C_2}{C_3}\frac{\partial \ln T_a}{\partial r}\right), \tag{70}$$

where

$$D_a = \frac{T_a}{\tau_{ab}\Omega_a^2 m_a}. \tag{71}$$

In a quasi-stationary state, the flux surface averaged impurity flux $\langle \Gamma_b \cdot \nabla r\rangle$ is related to the corresponding main ion flux $\langle \Gamma_a \cdot \nabla r\rangle$ by the ambipolarity condition

$$e_a \langle \Gamma_a \cdot \nabla r\rangle + e_b \langle \Gamma_b \cdot \nabla r\rangle = 0, \tag{72}$$

because of the momentum conservation during the unlike-species collisions. The constraint in Eq. (72) is also consistent with the quasi-neutrality requirement. Indeed, for a quasi-stationary state where the polarization current can be neglected, the total flux surface average neoclassical radial current has to be zero. Recalling that a Boltzmann electron response given by Eq. (64) yields a zero electron flux-surface average current, we obtain Eq. (72). Since for our simulations $\alpha = 1$, in the radial flux expression Eq. (70) we use transport coefficients for $Z_b = 1$, obtained in Sections 3.1 and 3.2 from the simulations with Abel collision operator C_A that was used to model like-species collisions in the Miller geometry simulations discussed in this section. Resulting predicted surface averaged particle flux profile $\langle \Gamma_a \cdot \nabla r\rangle$ agrees with results from the COGENT simulation, as illustrated in Fig. 5. The ion and impurity radial particle fluxes are related by ambipolarity Eq. (72) condition, as expected from analysis above. These results demonstrate the consistency of COGENT neoclassical simulations with theory [4] and results from slab geometry simulations discussed in Sections 3.1 and 3.2.

4. Conclusion

In this paper, we report on the implementation and testing of a model unlike-particle linearized collision operator in the gyrokinetic full-f continuum code COGENT. This operator is similar to the model operators for unlike-species collisions developed for delta-f simulations in Refs. [1,5] and it is based on the linearization of the Landau operator. However, consistent with the full-f formulation, the newly implemented operator also retains collisional thermalization of Maxwellian backgrounds for the case of different species temperatures. It conserves particle number, momentum,

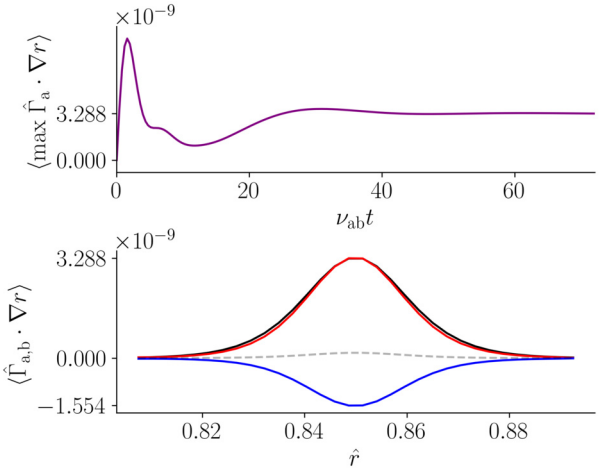

Fig. 5. (Top panel): Maximum of $\langle \hat{\Gamma}_a \cdot \nabla r\rangle$ along the radius plotted against time, showing the steady state. (Bottom panel) Radial profile of $\langle \hat{\Gamma}_a \cdot \nabla r\rangle$ is positive and shown in solid red curve, and is in good agreement with Eq. (70) shown with a black curve. The blue curve shows the radial profile of $\langle \hat{\Gamma}_b \cdot \nabla r\rangle$, and the gray dashed curve verifies the ambipolarity condition Eq. (72). Particle flux is normalized by $n_{a,0} v_{Ta}$, distance by $\tilde{l} = 1$ m. Simulated velocity grid is bounded by $|v_{||}|_{max}/v_{Ta} = 6$, $\mu_{max} B/T_a = 6$. Domain resolution is $n_{v_{||}} = 96$, $n_\mu = 48$, $n_\theta = 32$, $n_r = 32$.

and energy of colliding species, is self-adjoint for equal background temperatures of colliding species, and preserves the velocity dependence of the Coulomb mean free path. The latter property is critically important to recover the thermal force from the unlike-species collisions. The model operator is tested in simulations of parallel plasma transport in a uniform slab geometry by considering a large species mass ratio ($m_a/m_b = 100$) and a strongly-collisional regime. This problem is analogous to the electron-ion transport problem analyzed by Braginskii, and we analyze our simulation results by using the Braginskii model. For the case where like-particle collisions within the light species are modeled with the Fokker-Planck operator, the parallel transport coefficients obtained in the COGENT simulations are within $3-6\%$ of the corresponding Braginskii's results. When we replace the Fokker-Planck operator with the previously implemented Abel linearized operator for self-collisions, we obtain coefficients within 20% of Braginskii's results. In addition, we verify the Onsager symmetry of the transport coefficients, which follows from the self-adjointness property of the collision model for equal background temperatures. Finally, we simulate the Pfirsch-Schlüter problem of the radial ion-heavy impurity transport in a toroidal geometry, and recover the theoretical expression [4] for radial neoclassical fluxes in terms of parallel transport coefficients.

The ability of the implemented operator to recover the thermal force is important for simulating experimentally relevant plasma, since this force is widely recognized [3,15,16] to play one of the major roles in impurity transport in a tokamak edge. We, however, note that an ion distribution function can substantially deviate from a Maxwellian background in a steep edge region (e.g., under H-mode conditions), which affects the applicability limits of the linearized collision model. Our future work will focus on extending the COGENT's full Fokker-Planck operator to support unlike-species with an arbitrary mass ratio. This first-principle collision model will then be used to assess validity limits of the reduced collisional model reported here.

Declaration of competing interest

The authors declare that they have no known competing financial interests or personal relationships that could have appeared to influence the work reported in this paper.

Data availability

The data generated and analyzed in this study will be made available upon reasonable request.

Acknowledgements

This work was supported by the U.S. Department of Energy, Office of Science, Office of Fusion Energy Sciences under Award No. DE-SC0016548 at UCSD, and under Contract No. DE-AC52–07NA27344 at LLNL.

References

[1] R. Kolesnikov, W. Wang, F. Hinton, J. Comput. Phys. 229 (2010) 5564.
[2] M. Dorf, M. Dorr, Contrib. Plasma Phys. 60 (2020) e201900113.
[3] S. Braginskii, Consultants Bureau, New York, 1965.
[4] P.H. Rutherford, Phys. Fluids 17 (1974) 1782.
[5] H. Sugama, T.-H. Watanabe, M. Nunami, Phys. Plasmas 16 (2009) 112503.
[6] H. Sugama, S. Matsuoka, S. Satake, M. Nunami, T.-H. Watanabe, Phys. Plasmas 26 (2019) 102108.
[7] P. Donnel, X. Garbet, Y. Sarazin, V. Grandgirard, Y. Asahi, N. Bouzat, E. Caschera, G. Dif-Pradalier, C. Ehrlacher, P. Ghendrih, et al., Comput. Phys. Commun. 234 (2019) 1.
[8] P. Crandall, D. Jarema, H. Doerk, Q. Pan, G. Merlo, T. Görler, A.B. Navarro, D. Told, M. Maurer, F. Jenko, Comput. Phys. Commun. 255 (2020) 107360.
[9] M. Francisquez, J. Juno, A. Hakim, G.W. Hammett, D.R. Ernst, J. Plasma Phys. 88 (2022) 905880303.
[10] P. Ulbl, D. Michels, F. Jenko, Contrib. Plasma Phys. 62 (2022) e202100180.
[11] B. Frei, S. Ernst, P. Ricci, Phys. Plasmas 29 (2022) 093902.
[12] L. Landau, Phys. Z. Sowjetunion 10 (1936) 154–164.
[13] R. Hager, E. Yoon, S. Ku, E.F. D'Azevedo, P.H. Worley, C.-S. Chang, J. Comput. Phys. 315 (2016) 644.
[14] M. Dorf, R. Cohen, M. Dorr, J. Hittinger, T. Rognlien, Contrib. Plasma Phys. 54 (2014) 517.
[15] P.C. Stangeby, CFFTP-G–9042, 1990.
[16] S. Yamoto, Y. Homma, K. Hoshino, M. Toma, A. Hatayama, Comput. Phys. Commun. 248 (2020) 106979.
[17] R. Miller, M. Chu, J. Greene, Y. Lin-Liu, R. Waltz, Phys. Plasmas 5 (1998) 973.
[18] M. Dorf, M. Dorr, J. Hittinger, R. Cohen, T. Rognlien, Phys. Plasmas 23 (2016) 056102.
[19] M. Dorf, M. Dorr, Contrib. Plasma Phys. 58 (2018) 434.
[20] M. Dorf, M. Dorr, Contrib. Plasma Phys. 60 (2020) e201900113.
[21] A.S. Richardson, 2019 NRL plasma formulary, Tech. Rep, US Naval Research Laboratory, 2019.
[22] B.A. Trubnikov, Review of Plasma Physics, edited by M. A. Leontovich, Vol. 1, Consultants Bureau, New York, 1965.
[23] E. Belli, J. Candy, Plasma Phys. Control. Fusion 54 (2011) 015015.
[24] Q. Pan, D.R. Ernst, P. Crandall, Phys. Plasmas 27 (2020) 042307.
[25] R. Kolesnikov, W. Wang, F. Hinton, G. Rewoldt, W. Tang, Phys. Plasmas 17 (2010) 022506.
[26] F.L. Hinton, Handbook of Plasma Physics, vol. 1, 1983, p. 331.
[27] D. Estève, X. Garbet, Y. Sarazin, V. Grandgirard, T. Cartier-Michaud, G. Dif-Pradalier, P. Ghendrih, G. Latu, C. Norscini, Phys. Plasmas 22 (2015) 122506.
[28] D. Gray, J. Kilkenny, Plasma Phys. 22 (1980) 81.
[29] M. Dorf, R. Cohen, M. Dorr, T. Rognlien, J. Hittinger, J. Compton, P. Colella, D. Martin, P. McCorquodale, Phys. Plasmas 20 (2013) 012513.
[30] I. Abel, M. Barnes, S. Cowley, W. Dorland, A. Schekochihin, Phys. Plasmas 15 (2008) 122509.
[31] H. Dreicer, Phys. Rev. 117 (1960) 329.
[32] P.L. Bhatnagar, E.P. Gross, M. Krook, Phys. Rev. 94 (1954) 511.
[33] A. Lenard, I.B. Bernstein, Phys. Rev. 112 (1958) 1456.
[34] J. Dougherty, Phys. Fluids 7 (1964) 1788.
[35] G. Dif-Pradalier, P. Diamond, V. Grandgirard, Y. Sarazin, J. Abiteboul, X. Garbet, P. Ghendrih, G. Latu, A. Strugarek, S. Ku, et al., Phys. Plasmas 18 (2011) 062309.
[36] V. Zhdanov, Transport Processes in Multicomponent Plasma, CPC Press, 2002.
[37] M. Dorf, M. Dorr, Phys. Plasmas 28 (2021) 032508.
[38] S. Novakovskii, C. Liu, R. Sagdeev, M. Rosenbluth, Phys. Plasmas 4 (1997) 4272.